Available online at www.worldscientificnews.com

World Scientific News

WSN 33 (2016) 67-78 EISSN 2392-2192

Synthesized and characterization of pure and Er^{+3} doped ZnO nanoparticles by using laser ablation in ethanol

Raid A. Ismail[1], Nadir F. Habubi[2,*], Esraa H. Hadi[2]

[1]Departement of Applied Sciences, The University of Technology, Baghdad, Iraq

[2]Physics Department, Education Faculty, University of Mustansiriyah, Baghdad, Iraq

*E-mail address: nadirfadhil@uomustansiriyah.edu.iq

ABSTRACT

Pulsed laser ablation in ethanol at room temperature with laser fluence 4.62 J/cm^2 was employed to synthesize pure zinc oxide (ZnO) and Er- doped ZnO nanocolloidal suspension. The structural properties were determined by using x-ray diffraction (XRD) method and was confirmed its hexagonal wurtzite structure. The photoluminescence spectra (PL), AFM and FTIR measurement of the synthesized pure and Er-doped ZnO is carried out. The photoluminescence spectra measurements show that all the samples have ultraviolet emission and green emission and the surface granular morphology. The FTIR spectra indicate the existence of Zn-O, Er-O-Er and Er-O stretching modes. Al/ZnO/P-Si/Al and Al/Er-ZnO/P-Si/Al photodetectors hetrojunction has two peaks of response located at 650 nm for and 790 nm and the first peak shifted to 550nm for the doped hetrojunction with max sensitivity ≈ 0.7A/W. The maximum specific detectivity is 4.3×10^{12} $W^{-1}\cdot cm\cdot Hz^{-1}$ and 3×10^{12} $W^{-1}\cdot cm\cdot Hz^{-1}$ for undoped and doped hetrojunctions respectively. The values of the built-in potentials 0.9 volt for Al/ZnO/P-Si/Al heterojunction and 0.6 volt for Al/Er-ZnO/P-Si/Al hetrojunction.

***Keywords*:** Zinc Oxide; AFM; XRD; Er doping; nanocollidal suspension; Heterojunction

1. INTRODUCTION

Zinc oxide, one of the most promising material, has been demonstrated to be applicable in solar cells [1,2], light-emitting diodes [3,4], room temperature ultraviolet lasers [5], gas sensor [6], field-effect transistors [7] and piezoelectric-gated diode [8]. It has attracted increasing interest in fabricating ZnO structures with designed morphology and properties while the desired optical and electrical properties could be achieved by doping ZnO with various elements. Introduction of impurity atoms is the most widely adopted method to tune the magnetic, electrical and optical properties of materials [9]. The Er-doped semiconductors are the potential optoelectronic materials [10-13] due to the Er intra-4f shell transition with a photoemission at a wavelength of 1.54 μm, which lies in the minimum loss region of silica based optical fibers [10,14].

Zinc oxide is chosen to be the host semiconductor [15-17], not only due to the wide band gap which can be applicable to the excitation of Er, but also the controllable electrical conductivity [18]. Up to now, physical doping methods, such as ion implantation [19], laser ablation [16], and high temperature calcinations [15,20], have mainly been used to introduce Er into ZnO substrate. Recently, pure and Er^{3+} -doped ZnO have been fabricated using laser ablation in liquid (ethanol). The structural, Atomic force microscopy (AFM), FTIR measurements and Photoluminescence (PL) emission spectra of the pure ZnO and Er^{3+} -doped ZnO was investigated.

2. EXPERIMENTAL

Laser ablation of a pure ZnO and Er-ZnO plates in ethanol at room temperature has been conducted using the (1064 nm) Nd:YAG yttrium aluminum garnet laser (type HUAFEI), operating with a pulse duration of 10 ns and a repetition rate of 10 Hz. The zinc target (purity of 99.99% provided from Ludeco) and doping with Er_2O_3 taken from SPEX INDUSTRIES, INC. METHUCHEN, NJ08840, USA) with high purity (99.999%) was fixed at bottom of quartz vessel containing of 5 ml of ethanol. The laser power fluence 4.62 J/cm^2 using focused lens of 11cm and the beam spot size 2.37 mm and the ablation time has been maintained at 5 min. The crystal structure properties were examined by X-ray diffraction (XRD-6000, Shimadzu X-ray diffractometer) using Cu Kα line. The surface roughness and topography observed by Atomic Force Microscopy (AFM). The photoluminescence (PL) in the solution was measured at room temperature with an excitation source of wavelength of (350 nm) and The (SHIMADZU- 8400S) Scan of the FTIR measurements is performed over the range between 400-4000 cm^{-1} for the prepared sample.

3. RESULTS AND DISCUSSION

The XRD pattern of the pure and Er-doped ZnO nanoparticles formed by laser ablation in ethanol at room temperature displayed in Fig. 1 reveals that they are polycrystalline and possess the hexagonal wurtzite structure and no impurity phase related to Er^{3+} could be found. The diffraction peaks shift to lower angle slightly with the Er-ZnO. The crystallite size has also been calculated using Scherrer's formula [21,22].

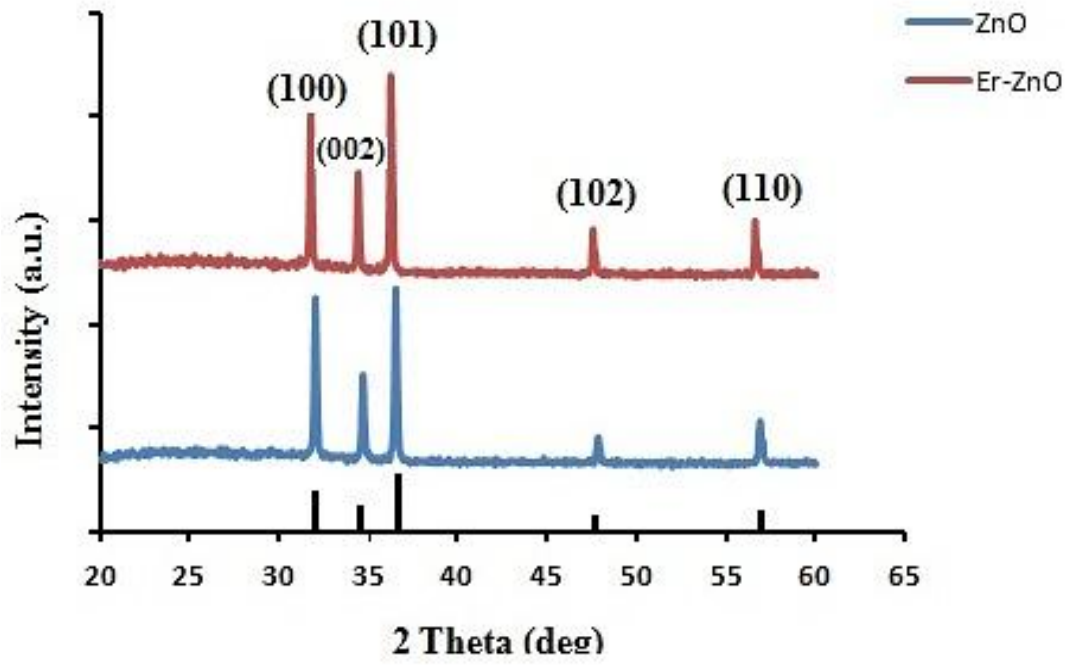

Fig. 1. XRD pattern for ZnO and Er-ZnO nanoparticles films ablated in ethanol at 4.62 J/cm^2 laser fluence.

The average grain size D was found and listed in Table (1).

$$D = \frac{K\lambda}{\beta.\cos(\theta)} \qquad (1)$$

where the β is the full width at the half maximum of the characteristic spectrum in units of radians and K is the Scherrer constant (1 > K > 0.89).

The average grain size of ZnO and Er-ZnO particles was found to be around 50.083 and 54.091 nm from XRD analysis. This difference in grain size can be ascribed to the difference in the lattice constants obtain. The strain value δ and the dislocation density η can be evaluated by using the following relations [21, 22], see Table 1:

$$\delta = \frac{1}{D^2} \qquad (2)$$

$$\eta = \frac{\beta.\cos(\theta)}{4} \qquad (3)$$

The results revealed that the strain and dislocation density are decreasing with the increasing grain size.

Table 1. Summary of X-ray characterization.

Laser fluences (J/cm^2)	Samples	2 θ (deg)	hkl Plane	d observe (Å)	FWHM (deg)	D (nm)	$\delta \times 10^{14}$ lines·m^{-2}	$\eta \times 10^{-4}$ $lines^{-2}$·m^{-4}
4.62	ZnO	36.3361	(101)	2.47045	0.1538	54.091	3.4178	6.4059
		31.8511	(001)	2.80734	0.1574	52.217	3.66759	6.6359
		34.504	(200)	2.59732	0.1593	51.955	3.70466	6.6693
	Er-ZnO	36.556	(101)	2.4437	0.1659	50.178	3.9716	6.90540
		32.08	(001)	2.7737	0.1642	50.083	3.9867	6.91849
		34.733	(200)	2.5677	0.1559	53.121	3.5437	6.52281

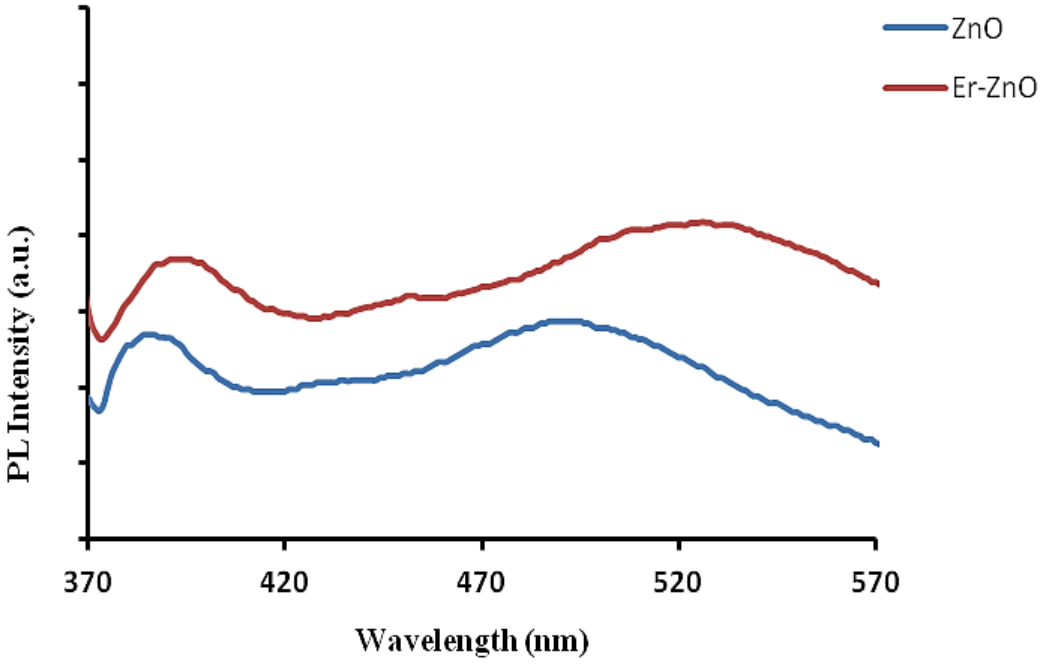

Fig. 2. PL spectra of pure ZnO and Er-doped ZnO ablated in ethanol at 4.62 J/cm^2 laser fluence.

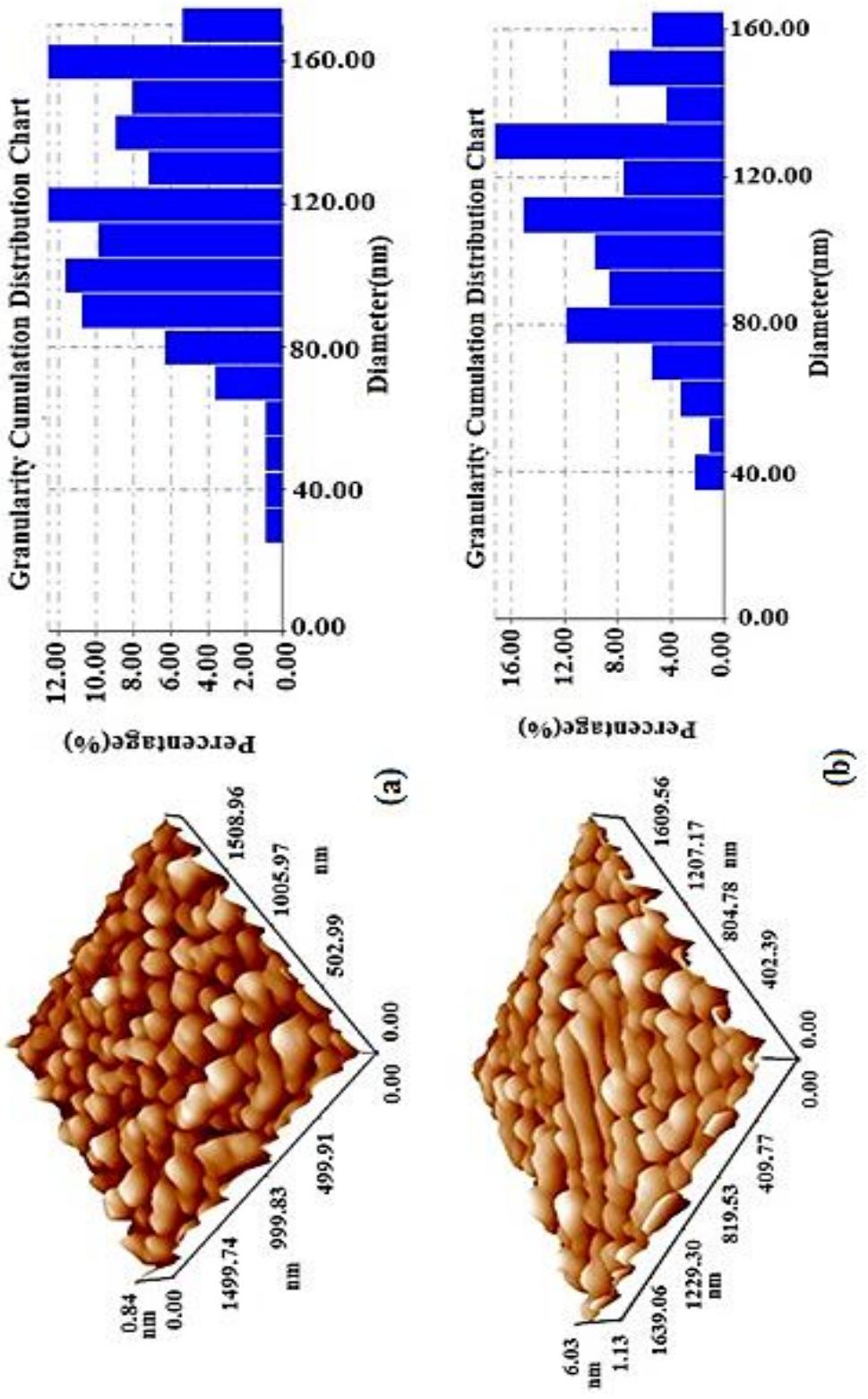

Fig. 3. The AFM images for (a) pure and (b) Er-doped ZnO nanoparticles ablated in ethanol at 4.62 J/cm^2 laser fluence.

PL spectra of the pure and Er-doped ZnO nanoparticles excited by 350 nm at room temperature is shown in Fig. 2. The PL spectra of ZnO nanorods contain a strong UV emission (NBE) peak at around 382 nm. Besides, a relatively weak and broad green band occurred. The UV emission is originated from excitonic recombination [23,24] corresponding to the nearest band-edge emission of ZnO. The green emission peak is commonly referred to deep-level or trap-state emission [21,25]. Various mechanisms have been proposed for the visible light emission of ZnO. Oxygen vacancies occur in three different charge states: the neutral oxygen vacancy (VO), the singly ionized oxygen vacancy (VO*), and the doubly ionized oxygen vacancy (VO**). The strong UV and weak green bands imply good crystal surface [26]. The shift in peak position of PL may be due to different size of nanoparticles produced and attributed to quantum-confinement induced energy gap enhancement.

The surface morphology of pure ZnO and Er-ZnO Nanparticles colloidal prepared by pulse laser ablation in ethanol was obtained using atomic force microscopic images. Fig. 3 shows the particle size distribution and nanoparticles topography of dried colloids prepared at 4.62 J/cm^2 laser fluence. The surface morphology, and hence particle size distribution also the values of the root mean square and surface roughness are recognized and listed in Tables 2. Figure (3a) exhibits granular morphology with a regular arrangement of aggregates of nanocrystals for pure ZnO film. Fig. 4b, it is evident that Er-doped film is formed by large clusters/grains due to the agglomeration.

The columnar arrangement of grains seen in 3D image Fig. 4a and b, shows the growth along the c-axis direction perpendicular to the substrate surface and The grains are basically round.

Table 2. Grain size, roughness average and Root mean square of pure and Er-doped ZnO nanoparticles ablated in ethanol.

Laser Fluence (J/cm^2)	Samples	Grain size (nm)	Roughness average (nm)	Root Mean square (nm)
4.62	ZnO	97.55	0.118	0.148
	Er-ZnO	104.13	0.868	1.111

Figure (4) gives the FTIR result for Er-ZnO NPs prepared at 1.06 μm laser wavelength with a constant laser fluence of (4.62 J/cm^2).In this figure we could recognize the transition peaks at (439.77,516.92, 594.08,408. 91,516.92) cm^{-1} wave number which relates to the stretching vibrations mode of the Zn-O band [27]. The transition peaks at 415, 471 cm^{-1} and (563, 670) cm^{-1} wave number is related to the stretching modes of the Er–O band and Er–O–Er band respectively. Transition peaks at (3000, 3564.45, 3865.35, 1481.33) cm^{-1} are related to the harmonics of H–OH stretching modes. Many other peaks appear at 717.52, 972.12, 825.53, 894.97, 856.39, 686.66, 624.94 cm^{-1} wave number is related to symmetrical stretching mode and bending mode of the C-H-H bands respectively.

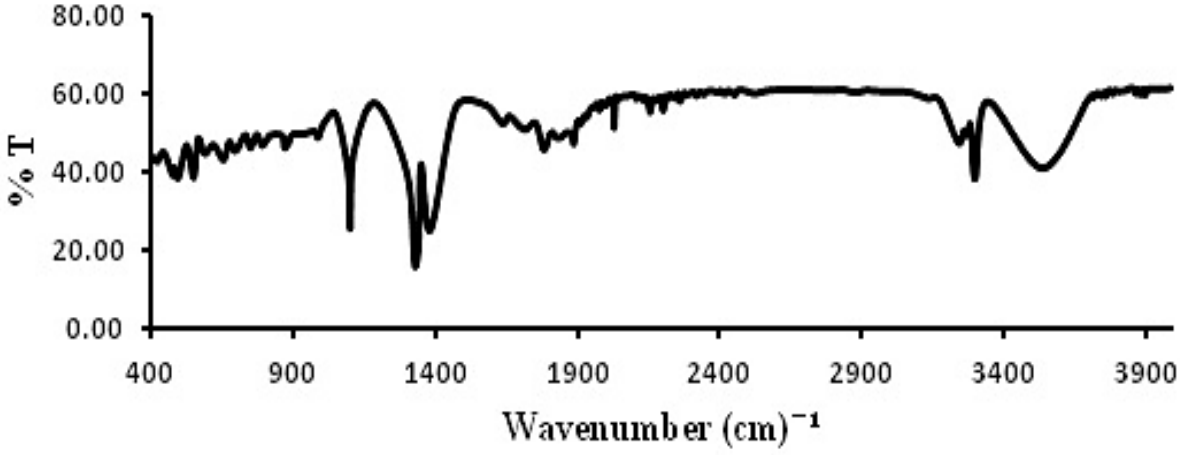

Fig. 4. FTIR spectra of Er-doped ZnO nanoparticles ablated in ethanol at 4.62 J/cm^2 laser fluence.

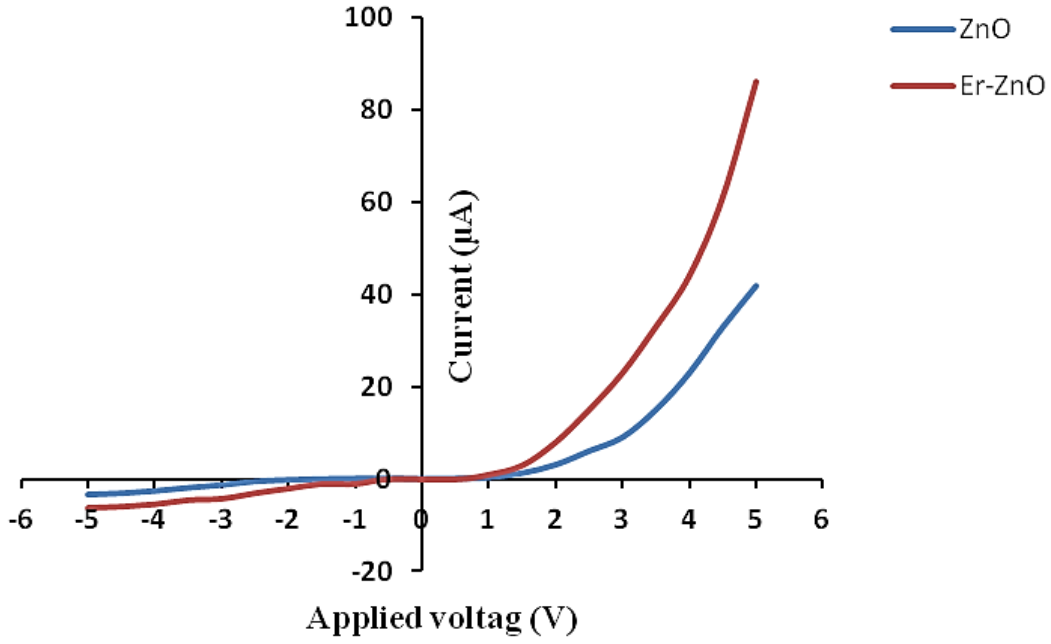

Fig. 5. Dark Current-Voltage for ZnO/Si and Er-ZnO/Si heterojunctions at **4**.62 J/cm^2 laser fluence.

The electrical behavior of Al/ZnO/p-Si/Al and Al/Er-ZnO/p-Si/Al such as Schottky or heterojunction is determined generally by depending on the characteristics of current-voltage characteristics. Figure 5, shows the dark I-V characteristics in forward and reverse directions of Al/ZnO/p-Si/Al and Al/Er-ZnO/p-Si/Al sandwich structure prepared at 4.62 J/cm^2 laser fluence measurements carried out by applying voltage supplied to the sample from -5+5 V.

Under the forward bias for the voltage great than 1V it shows the exponential increase in current due to decrease in the depletion layer width at ZnO/p-Si and Er-ZnO/p-Si interfaces and slightly increase for the voltage less than 1V also the figure shows that the current increases reaching to 86 μA for doped sample. Under reverse bias, reverse current very small less than 6.5 μA produce from high resistance in the reverse bias.

Capacitance-voltage measurement is one of the most important methods for obtaining information about the built-in potential, depletion width, and junction type. Figure 6, shows C^{-2} –V of ZnO/p-Si and Er-ZnO/p-Si heterojunctions in dark at room temperature and at the increment voltage of frequency 100 kHz. This plot shows a linear relationship of C^2 with bias voltage indicating that these junctions are an abrupt type, and also shows that the junction capacitance is inversely proportional to the bias voltage for Al/ZnO/p-Si/Al and Al/Er-ZnO/p-Si/Al. Built in potential (V_{bi}) can also calculate by extrapolating ($1/C^2$-V), plot to ($I/C^2 = 0$). The values of the built-in potentials for heterojunctions decrease with the dopant. The value (0.6 volt and 0.9 volt) for doped and undoped junctions respectively. There is a decrease in the capacitance at strong bias and this reduction in the capacitance may be attributed to the increased conductivity at strong dc bias. The reduction in the junction capacitance with increasing the bias voltage results from the expansion of the depletion layer with the built-in potential.

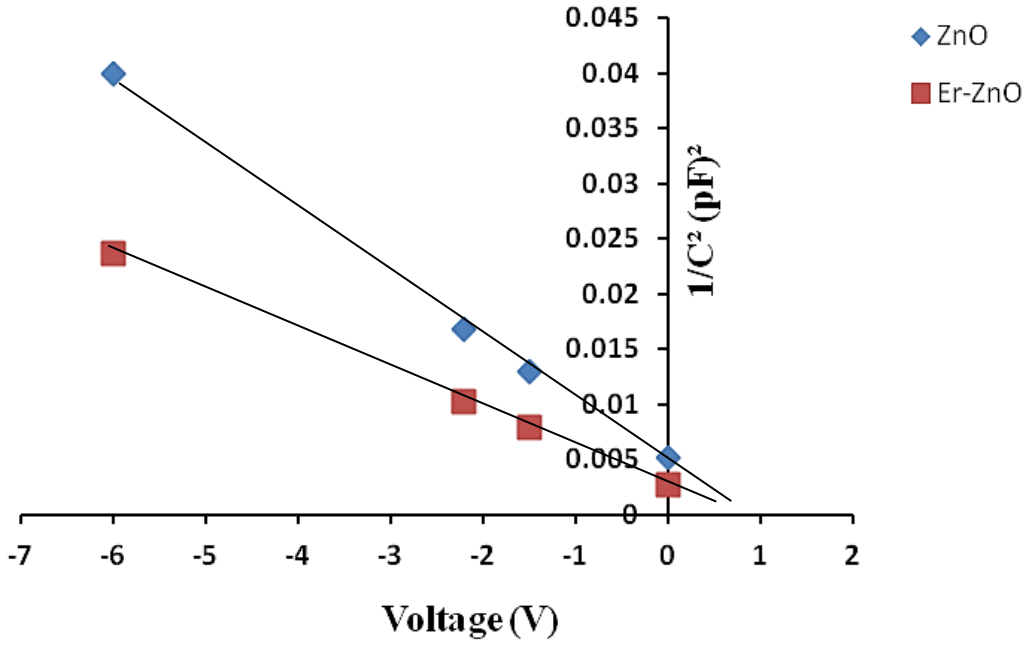

Fig. 6. $1/C^2$-V plot for ZnO/Si and Er-ZnO/Si heterojunctions at 4.62 J/cm^2 laser fluence.

The responsivity is an important parameter that is usually specified by the manufacturer knowledge of the responsivity allows the user to determine how mach detector signal will be available for a specific application. The responsivity is given by [28]:

$$R_\lambda = \frac{I_{Ph}}{P_{in}} \quad \text{(A/W)} \qquad (4)$$

where: I_{ph} *is* the photocurrent and P_{in} is the input power.

The spectral responsivity of structures is investigated in the wavelength range of (400-900) nm with 5V as shown in Figure 7. Figure 7, shows that the spectral responsivity curve of ZnO/p-Si and Er-ZnO/p-Si consists of two peaks of response, the first peak is located at 650 nm due to the absorption edge of ZnO nanoparticles, while the second region is located at 790 nm due to absorption edge of silicon for ZnO/p-Si. The first peak is shifted to the 550 nm for the Er-ZnO/p-Si due to the Er doped ZnO, while the second region remains at the same (790 nm) due to this region relate to absorption edge of silicon.

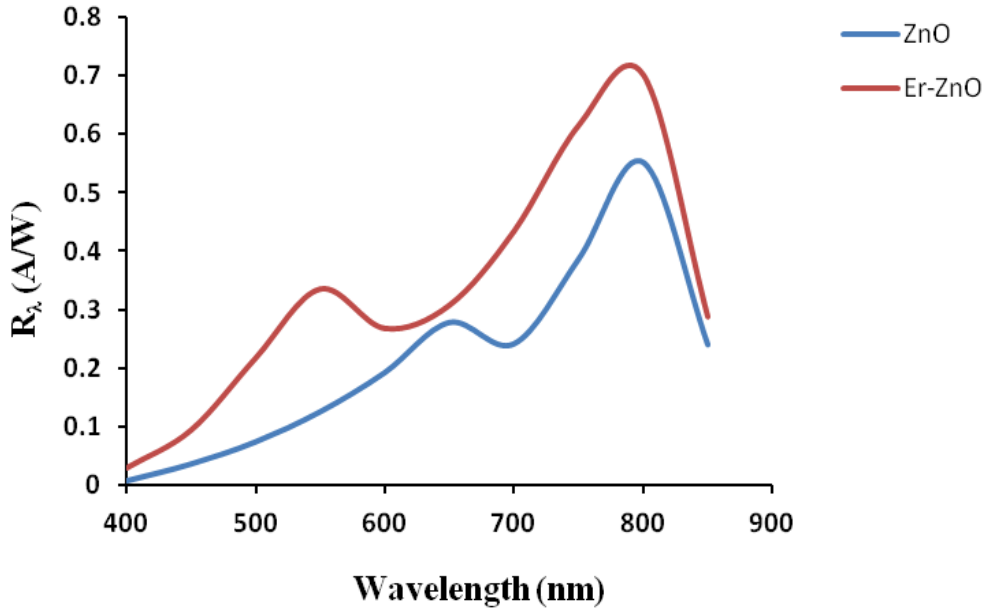

Fig. 7. Responsivity for ZnO/Si and Er-ZnO/Si heterojunctions at 4.62 J/cm^2 laser fluence.

Specific detectivity (D*) is the importance parameters for photodetector which represented a minimum detectable power, therefore; the performance of the detector is linked with this parameter and given by [29,30]:

$$D_\lambda = \frac{R_\lambda}{I_n} \qquad (5)$$

where I_n: is noise current

Figure 8, shows that the specific detectivity as a function of wavelength for ZnO/p-Si and Er-ZnO/p-Si Photodetectors. This figure shows that the detectivity depend directly on responsivity.

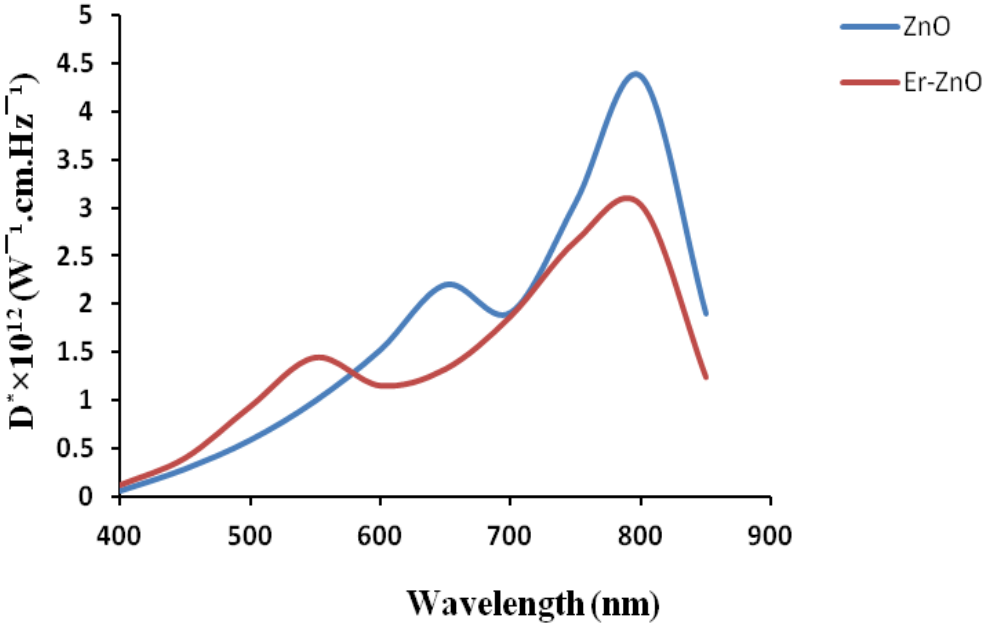

Fig. 8. Detectivity for ZnO/Si and Er-ZnO/Si heterojunctions at 4.62 J/cm^2 laser fluence.

4. CONCLUSION

The structural, morphological, and the photoluminescence spectra properties of pure ZnO and Er-doped ZnO NPs colloid at room temperature prepared by Nd:YAG laser ablation in ethanol method is investigated. XRD spectra indicate that all the films exhibit wurtzite hexagonal crystal structure. The photoluminescence spectra measurements show that all the samples have ultraviolet emission centered at 382 nm and green emission. The surface morphology is investigated by atomic force microscopic. The results show that the surface granular morphology with a regular arrangement of aggregates of nanocrystals. The FTIR spectra indicate the existence of the distinct characteristics transition peak for Zn-O stretching modes and Er-O-Er, Er-O stretching modes. The current increases with doped ZnO reaching to 86 μA. Under reverse bias, reverse current very small less than 6.5 μA produce from high resistance in the reverse bias. The reduction in the junction capacitance with increasing the bias voltage. The spectral responsivity curve of ZnO/p-Si and Er- ZnO/p-Si consists of two peaks of response the first peak related with ZnO and the second peak related with the silicon and that the detectivity depend directly on responsivity.

References

[1] H. Rensmo, K. Keis, H. Lindström, S. Södergren, A. Solbrand, A. Hagfeldt, S. E. Lindquist, L. N. Wang, and M. Muhammed, *J. Phys. Chem. B* 101, 2598 (1997).

[2] M. Law, L. E. Greene, J. C. Johnson, R. Saykally, and P. D. Yang, *Nature Mater.* 4, 455 (2005).

[3] D. K. Hwang, S. H. Kang, J. H. Lim, E. J. Yang, J. Y. Oh, J. H. Yang, and S. J. Park, *Appl. Phys. Lett.* 86, 222101 (2005).

[4] J. H. He, S. T. Ho, T. B. Wu, L. J. Chen, and Z. L. Wang, *Chem. Phys. Lett.* 435, 119 (2007).

[5] M. H. Huang, S. Mao, H. Feick, H. Yan, Y. Wu, H. Kind, E. Weber, R. Russo, and P. D. Yang, *Science* 292, 1897 (2001).

[6] H. Kind, H. Q. Yan, B. Messer, M. Law, and P. D. Yang, *Adv. Mater.* 14, 158 (2002).

[7] M. S. Arnold, P. Avouris, Z. W. Pan, and Z. L. Wang, *J. Phys. Chem.* B 107, 659 (2003).

[8] J. H. He, C. L. Hisn, J. Liu, L. J. Chen, and Z. L. Wang, *Adv. Mater.* 19, 781 (2007).

[9] L. E. Greene, B. D. Yuhas, M. Law, D. Zitoun, and P. D. Yang, *Inorg. Chem.* 45, 7535 (2006).

[10] A. Polman, *J. Appl. Phys.* 82, 1 (1997).

[11] S. Lanzerstorfer, L. Palmetshofer, W. Jantsch, and J. Stimmer, *Appl. Phys. Lett.* 72, 809 (1998).

[12] S. Coffa, G. Franzo, F. Priolo, A. Pacelli, and A. Lacaita, *Appl. Phys. Lett.* 73, 93 (1998).

[13] X. Zhao, S. Komuro, H. Isshiki, Y. Aoyagi, and T. Sugano, *Appl. Phys. Lett.* 74, 120 (1999).

[14] K. Takahei and A. Taguchi, *J. Appl. Phys.* 74, 1979 (1993).

[15] N. Mais, J. P. Reithmaier, A. Forchel, M. Kohls, L. Spanhel, and G. Muller, *Appl. Phys. Lett.* 75, 2005 (1999).

[16] S. Komuro, T. Katsumata, T. Morikawa, X. W. Zhao, H. Isshiki, and Y. Aoyagi, *J. Appl. Phys*. 88, 7129 (2000).

[17] M. Ishii, S. Komuro, T. Morikawa, and Y. Aoyagi, *J. Appl. Phys.* 89, 3679 (2001).

[18] J. H. He, C. S. Lao, L. J. Chen, D. Davidovic, and Z. L. Wang, *J. Am. Chem. Soc.* 127, 16376 (2005).

[19] J. Wang, M. J. Zhou, S. K. Hark, Q. Li, D. Tang, M. W. Chu, and C. H. Chen, *Appl. Phys. Lett.* 89, 221917 (2006).

[20] Z. Zhou, T. Komori, T. Ayukawa, H. Yukawa, M. Morinaga, A. Koizumi, and Y. Takeda, *Appl. Phys. Lett.* 87, 091109 (2005).

[21] H. Zeng, G. Duan, Y. Li, S. Yang, X. Xu, W. Cai, *Advanced Functional Materials* 20 (2010) 561-572.

[22] He´ le`ne Serier, Manuel Gaudon, Michel Me´ne´ trier, *Solid State Sciences*, 11 (2009) 1192-1197.

[23] Zhang X.T, Y.C. Liu, Z.Z. Zhi, J.Y. Zhang, Y.M. Lu, D.Z. Shen, G.Z.Z. Zhong, X.W. Fan and X.G. Kong. *J. Phys. D: Appl. Phys.*, 34 (2001) 27875.

[24] Alaoui Lamrani . M, M. Addou, Z. Sofiani, B. Sahraoui, J. Ebothé, A. El Hichou, N. Fellahi, J.C. Bernède, R. Dounia **,** *Optics Communications,* 277(1) (2007) 196-201.

[25] Xian-Hua Zhang, Jie Chen, Yaping Wu, Zhaoxiong Xie, Junyong Kang, Lansun Zheng, *Colloids and Surfaces A: Physicochem. Eng. Aspects*, 384 (2011) 580-584.

[26] Yang T, Li Y, Zhu MY, Li YB, Huang J, Jin HM, *Mater Sci Eng, B*, 170 (2010)129-132.

[27]. Deng, L. Li, J. H. Deng, Z. Liu, L. Xin "Synthesis and characterization of chitosan/ZnO nanoparticle composite Membranes". *Carbohydrate Research 345* (2010) 994-998, 2010.

[28] J.D. Vincent, Fundamentals of Infrared Detector Operating and Testing, John Wiley and Sons, New York, (1990).

[29] H. Kaube and F. Kmura, *Electronic Lett.* 13 (1971) 262-266.

[30]] R. D. Hudson, Infrared System Engineering, John Wiley and Sons, New York, (1969).

(Received 08 December 2015; accepted 21 December 2015)